Published in IET Communications
Received on 29th February 2008
Revised on 21st July 2008
doi: 10.1049/iet-com:20080124

ISSN 1751-8628

Analytical study of binary differential impulse radio-ultra wide band over single-mode fibre systems using two receiver structures

M. Jazayerifar[1] *J.A. Salehi*[1] *B. Cabon*[2]

[1]*Optical Networks Research Laboratory (ONRL), Electrical Engineering Department, Sharif University of Technology, Tehran, Iran*
[2]*Institute of Microélectronique, Electromagnétisme et Photonique (IMEP), UMR CNRS 5130 Centre National de la Recherche Scientifique, MINATEC-INPG, 3 parvis Louis Néel, BP257, Grenoble 38016 Cedex, France*
E-mail: mjazayerifar@yahoo.com

Abstract: A binary differential impulse radio-ultra wide band (IR-UWB) communication scheme over a single-mode optical fibre is examined. For a receiver structure, the conventional electrical receiver as well as an optical receiver structure, which is similar to the optical receiver used for digital, optically phase-modulated differential phase shift keying, are considered. The optical receiver can alleviate the IR-UWB receiver implementation challenges and it is studied for the first time in the context of IR-UWB. Considering various important noises, for example, phase noise, laser intensity noise, thermal noise and shot noise, analytical expressions for the error probability of the aforementioned receivers are derived. The mathematical models for optical components including laser diode and single-mode fibre, along with the analytical expressions for the receiver's error probability, are used to evaluate the overall performance of an UWB communication system over a fibre transmission medium. Furthermore, the electrical receiver is compared with the optical receiver and it is shown that the performance of the optical receiver can be as good as that of the electrical receiver and even better. The impact of wireless channel fading, bias current of laser diode and the coherence time of laser diode on the UWB over fibre system performance is also examined.

1 Introduction

Recently, impulse radio-ultra wide band (IR-UWB) communication systems are receiving considerable attention for short-range personal area networks. In IR-UWB systems, information bits are modulated on short-duration Gaussian pulses [1]. Low transmitted power of UWB signals limits the wireless range of these systems, and one way to extend the range is to use radio over fibre (RoF) systems. In RoF systems, analogue radio signals are modulated on the intensity of the optical signals and transmitted through a fibre-optic link. Owing to UWB signals, wide bandwidth and high data rate, RoF technology is an excellent alternative for UWB signal transmission. Transmission of IR-UWB signals through optical fibre has been a topic of interest for many researchers for the past few years, however most studies have focused on the feasibility and the experimental demonstration of such systems [2–4]. In this article, however, we consider a binary differential IR-UWB over fibre system which has not been examined previously in the literature. Differential IR-UWB systems are resistive to multipath fading and simple to implement [5]. In many applications where channel estimation poses major challenges in IR-UWB communication, employing differential IR-UWB could prove to be essential to overcome the aforementioned difficulties [5].

For our proposed differential IR-UWB signals over fibre, we consider two receiver structures: an electrical receiver and an optical receiver. The electrical receiver is a typical differential detector which is implemented by electrical circuits. The implementation of electrical receivers could be a challenging task because of the very short duration of IR-UWB signals. Several solutions based on pulsed multi-band and multi-band orthogonal frequency division

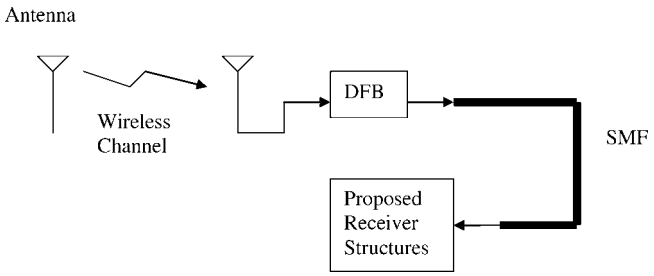

Figure 1 *Block diagram of a typical uplink UWB over fibre system using the proposed receiver structures in this paper*

multiplexing are proposed to alleviate this problem [6]. Implementing a segment of IR-UWB receiver in an optical domain can also alleviate the problem to some extent, especially in an RoF system. That is why, besides the electrical receiver, we have proposed an optical receiver for optical differential UWB systems. The optical detector proposed in this paper is in fact the receiver that is used for digital optically phase-modulated PSK systems [7], however in this paper it is used for an intensity-modulated UWB signal over fibre system. The proposed optical receiver can be used in the uplink of an UWB over fibre system.

We obtain analytical expressions for the error probability of the above two receivers. In our analysis, we consider the effect of various noise sources including laser intensity noise, phase noise, shot noise and thermal noise. Fig. 1 shows the block diagram of an optical uplink UWB over fibre system.

Considering this figure, we use mathematical models for optical components as well as the analytical expressions for error probability to evaluate the performance of the overall system. In this paper, a distributed feedback (DFB) laser is used to modulate UWB signals on optical power. The model of DFB is experimentally verified. We investigate the impact of DC component of the transmitted optical power and the coherence time of DFB laser on the performance of electrical and optical receivers and compare these two receivers.

The rest of this paper is organised as follows. In Section 2, the modulation scheme and receiver structures are described in more detail. In Section 3, mathematical models of the optical components are discussed. In Sections 4 and 5, the analytical expressions for the performance of the receivers are obtained. In Section 6, the performance of the whole system is evaluated and the numerical results are discussed. We conclude the paper in Section 7.

2 System description

In IR-UWB systems, data bits are modulated over short-duration Gaussian pulses which are represented by $s(t)$ in this paper. $s(t)$ could be either a monocycle or a doublet [1]

$$\text{Monocycle:}\quad s(t) \propto t \exp\left(-\left(\frac{t}{\tau}\right)^2\right) \tag{1}$$

$$\text{Doublet:}\quad s(t) \propto \left(1 - \frac{2t^2}{\tau^2}\right) \exp\left(-\left(\frac{t}{\tau}\right)^2\right) \tag{2}$$

In order to cover the whole UWB spectrum, that is, 3.1–10.6 GHz, the above wave forms must have a duration at about 200 ps [1].

At the transmitter, electrical UWB signals can be modulated on the optical carrier using either a laser diode or an external modulator. These components may affect the shape of the original electrical UWB signal. Let the transformed or reshaped UWB waveforms be represented by $u(t)$. We assume that the electrical current which modulates the DFB laser is $I(t) = I_b \pm I_{mod}\, s(t)$, where $s(t)$ is the normalised ideal UWB signal so that $\max[s(t)] - \min[s(t)] = 1$. I_b and I_{mod} are the bias current and modulating current, respectively. The corresponding optical power can also be considered as $P_o(t) = P_b \pm P_m\, u(t)$, where $u(t)$ is normalised so that $\max[u(t)] - \min[u(t)] = 1$. P_m and P_b are called the modulating power and bias power, respectively.

Note that in any differential modulation, the difference between the successive transmitted bits determines the value of the data bit, that is, two successive $P_o(t) = P_b + P_m\, u(t)$ or two successive $P_o(t) = P_b - P_m\, u(t)$ is detected as zero, whereas $P_o(t) = P_b + P_m\, u(t)$ followed by $P_o(t) = P_b - P_m\, u(t)$ or $P_o(t) = P_b - P_m\, u(t)$ followed by $P_o(t) = P_b + P_m\, u(t)$ is detected as 1. Considering this mapping, the two successive received bits must be multiplied to each other at the receiver.

In the following sections, we discuss the receiver structures needed to decode and obtain the above received signal.

2.1 Electrical receiver

The block diagram of the proposed electrical binary differential receiver is depicted in Fig. 2. The received optical signal is first transformed into an equivalent electrical domain signal and the rest of processing is applied in the electrical domain.

As shown in this figure, after photo-detection two successive bits are multiplied to each other and integrated over a bit duration to make the decision variable. This decision variable is compared with the threshold value (i_{th}) to detect the data bits.

2.2 Optical receiver

The block diagram of this receiver is shown in Fig. 3. The optical received signal is first passed through the optical structure shown in the left, and then it is photo-detected using a balanced photo-detector [7]. The receiver is made

doi: 10.1049/iet-com:20080124

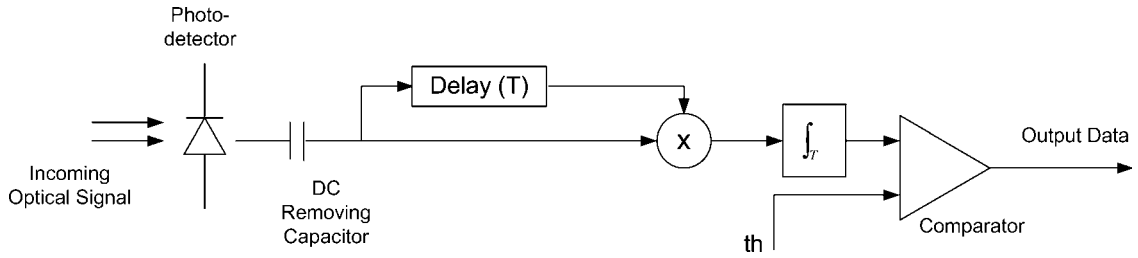

Figure 2 *Electrical binary differential receiver*

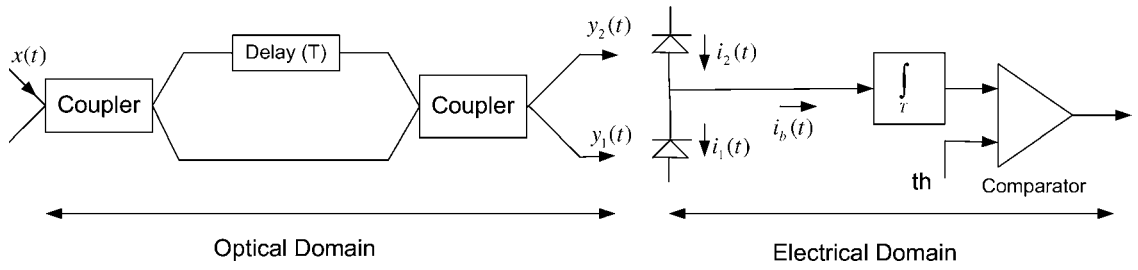

Figure 3 *Optical receiver for binary differential signals*

of a Mach–Zehnder interferometer and a dual-balanced photo-detector. Both of these equipments, that is, the Mach–Zehnder interferometer and the dual-balanced photo-detector, are conventional equipments and are frequently used in optical PSK receiver structures. The difference between the delay of the upper and lower interferometer lines must be equal to the bit duration. If the bit duration is large, a long fibre will be required to implement the delay and it makes the implementation and packaging of the differential phase shift keying receiver difficult. For example, if a 40-ns bit duration is used the required fibre length will be around 8 m which may prove difficult to implement but not impossible. However, In UWB systems the expected bit rate is around 500 Mb/s that corresponds to the bit duration of 2 ns. The fibre length required to implement this delay is around 40 cm which is considered practical for implementation purposes.

Note that implementation problems may result in receiver imperfections that affect the performance of receivers. For example, implementing a large delay may result in an inaccurate delay or even fluctuations of the delay value. However, in this paper we consider an ideal receiver, and all equations are derived based on this assumption.

Assume that $x(t)$ represents the optical electric field entering the receiver. Considering the figure above, the incident optical electric fields $y_1(t)$, $y_2(t)$ will be [8]

$$y_1(t) = \frac{1}{2}[-x(t) + x(t-T)],$$
$$y_2(t) = \frac{-\mathrm{j}}{2}[x(t) + x(t-T)] \quad (3)$$

where T represents the delay in Fig. 3 and is equal to a bit duration. The two photo-detectors shown in Fig. 3 release electric currents which are proportional to the square of the electric fields

$$i_1(t) = R|y_1(t)|^2, \quad i_2(t) = R|y_2(t)|^2 \quad (4)$$

where R is the responsivity of the photo-detector. From Fig. 3, we can write

$$i_\mathrm{b}(t) = i_2(t) - i_1(t) \quad (5)$$

Let $x(t) = A(t)\mathrm{e}^{-\mathrm{j}(\omega t + \varphi(t))}$, where $A(t)$ is the amplitude, ω and $\varphi(t)$ are the angular frequency and the phase of the optical field, respectively. Substituting $x(t) = A(t)\mathrm{e}^{-\mathrm{j}(\omega t + \varphi(t))}$ in (3)–(5) we obtain

$$i_\mathrm{b}(t) = R[A(t)A(t-T)\cos(\varphi(t) - \varphi(t-T))] \quad (6)$$

In the above equation, the amplitude of the optical electric field of two successive bits is multiplied. Furthermore, from Fig. 3 the decision variable, which is denoted by D_v, is equal to the integration of this multiplication over a bit duration, that is, $D_\mathrm{v} = \int_0^T i_\mathrm{b}(t)\mathrm{d}t$.

Note that in (6) the term $\cos(\varphi(t) - \varphi(t-T))$ is affected by both the laser chirp effect and the laser phase noise. The first effect, that is, laser chirp effect, is advantageous in differential UWB over fibre systems, and the second effect, that is, laser phase noise, is disadvantageous as will be discussed in later sections.

3 Optical components modelling

Considering Fig. 1, we develop mathematical models for DFB laser diode and single-mode fibre (SMF) [9]. In modelling the SMF, the effect of dispersion and attenuation is considered [10], and the nonlinear effects and polarisation mode dispersion are not taken into account because of their negligible effect in our application [9]. Laser rate equations are used to model the DFB laser. We have assumed a single-mode case. Laser rate equations are based on nine parameters that explain various aspects of laser diode behaviour [11]. In order to determine the numerical values of these parameters, a curve-fitting approach is used [11]. The small signal frequency response of a DFB laser is experimentally measured. It can also be theoretically expressed in terms of the laser rate equation parameters [11]. We employ those numerical values for rate equation parameters that make the theoretical frequency response to become the best fit when compared with the experimental measurement results as shown in Fig. 4. In order to obtain those values, we use numerical optimisation methods [9]. We set an upper and lower bound for each parameter, so that the optimisation leads to proper numerical values. Using the obtained numerical values, we also compare the static $L-I$ (light power–current) characteristic of the laser with the experimental results, and we find that they are in very good agreement, and the DFB threshold current is $I_{th} = 10$mA as shown in Fig. 5. The numerical values for DFB laser rate equation parameters are presented in Table 1.

Note that the actual DFB laser model is obtained by inserting the numerical values of Table 1 in the laser rate equations used in [11]. The models of this section are used to obtain $u(t)$ from $s(t)$ as explained in Section 2.

4 Electrical receiver performance evaluation

Assuming an additive noise model [10], the photo-detected current will be

$$i(t) = RP_o(t) + N(t) \tag{7}$$

where R is the responsivity of the photo-detector, $P_o(t)$ is the incident optical power and $N(t)$ represents the noise. We consider the impact of intensity noise, shot noise and thermal noise whose variances are $R^2P_o^2(t)(\text{RIN})$, $eRP_o(t)$ and $2kT_r/r$ [10] and will be represented by σ_P^2, σ_s^2 and σ_t^2, respectively. Here, RIN represents the relative intensity noise of laser, e is the electron charge, k is the Boltzman constant, T_r is the absolute temperature and r is the electrical resistance. The mean of $N(t)$ is equal to zero. We assume that all noise are white. Therefore considering the independence of noises, we can write the covariance function of $N(t)$ as

$$C_N(t, \tau) = \left(R^2P_o^2(t)(\text{RIN}) + eRP_o(t) + \frac{2kT_r}{r}\right)\delta(\tau) \tag{8}$$

From Fig. 2, the decision variable, D_v, is

$$D_v = \int_0^T (i(t) - i_{DC})(i(t-T) - i_{DC})\mathrm{d}t \tag{9}$$

where i_{DC} represents the DC component of the released current. This DC component has no information and is removed prior to obtaining the decision variable D_v as shown in Fig. 2.

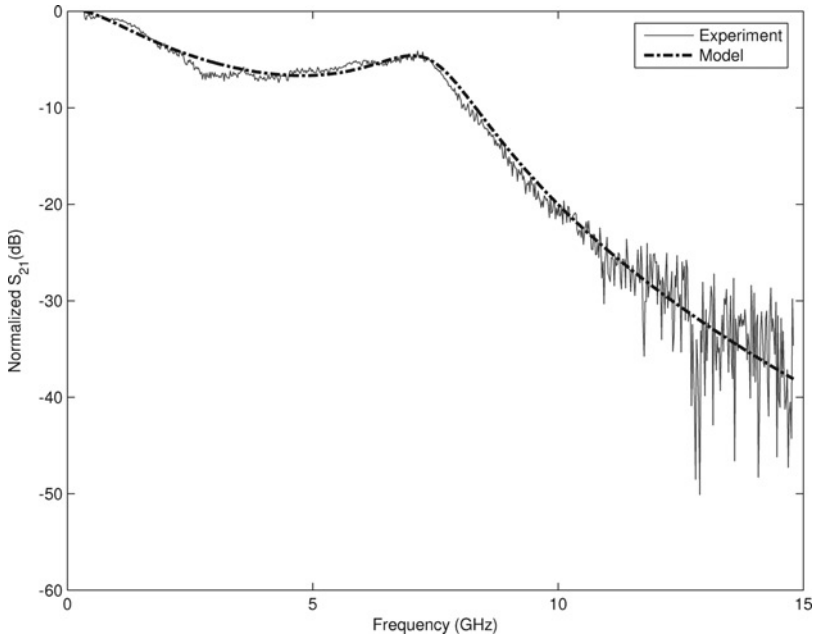

Figure 4 *Small signal frequency response of DFB in $I_b = 50$ mA*

doi: 10.1049/iet-com:20080124

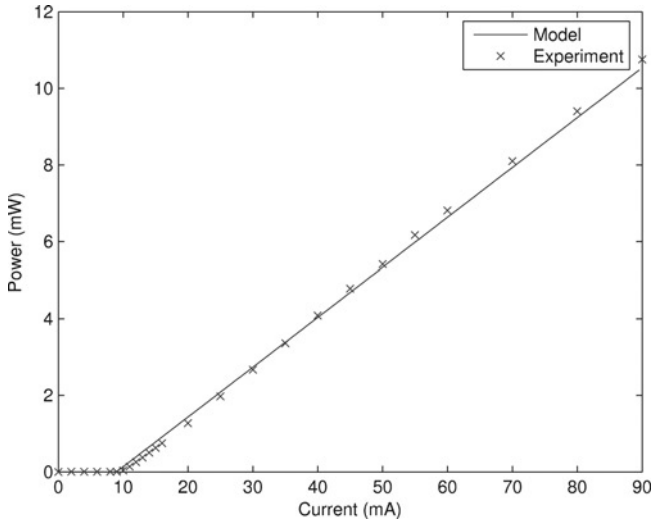

Figure 5 *Light–current (L–I) static characteristic of DFB laser*

Table 1 Laser rate equation parameters

mode confinement factor	Γ	0.2851
gain slope constant, cm^3/s	g_0	9.465×10^{-7}
active layer volume, cm^3	V	2.315×10^{-11}
carrier density at transparency, cm^{-3}	N_t	1.1569×10^{-18}
gain compression factor, cm^3	ε	2.0371×10^{-17}
the fraction of spontaneous emission coupled into the lasing mode	β	1.1246×10^{-4}
photon lifetime, ps	τ_p	2.1263
electron lifetime, ns	τ_e	1.1937
differential quantum efficiency	η_0	0.3316

Assume that the mean and the variance of D_v is represented by η and σ^2, respectively. Then from (7) and (9) they can be obtained after some straightforward algebra

$$\eta = R^2 \int_0^T (P_o(t) - P_b)(P_o(t-T) - P_b)\mathrm{d}t \tag{10}$$

where P_b represents the DC component of the optical power at the receiver as explained in Section 2. Considering (7)–(9), the variance of D_v is also obtained after a straightforward algebra

$$\sigma^2 \simeq \int_0^T R^2(P_o(t) - P_b)^2 W(t-T)\mathrm{d}t + \int_0^T R^2(P_o(t-T) - P_b)^2 W(t)\mathrm{d}t \tag{11}$$

where

$$W(t) = \left(R^2 P_o^2(t)(\mathrm{RIN}) + eRP_o(t) + \frac{2kT_r}{r}\right) \tag{12}$$

Assume that $P_o(t) = P_b \pm P_m u(t)$, as stated in Section 2. Now we can simply obtain the error probability. If the data bit is zero, the corresponding transmitted bits may be either $P_o(t) = P_b + P_m\ u(t)$, $P_o(t-T) = P_b + P_m u(t)$ or $P_o(t) = P_b - P_m u(t)$, $P_o(t-T) = P_b - P_m u(t)$. Substituting the above expressions in (10)–(12) we obtain the decision variable's mean and variance which are represented by $\eta_{0,1}$, $\sigma^2_{0,1}$ and $\eta_{0,2}$, $\sigma^2_{0,2}$, where the indices (0,1) and (0,2) represent the first and the second cases, respectively. If the data bit is 1, the corresponding transmitted bits may be either $P_o(t) = P_b + P_m\ u(t)$, $P_o(t-T) = P_b - P_m u(t)$ or $P_o(t) = P_b - P_m u(t)$, $P_o(t-T) = P_b + P_m u(t)$. Both of them lead to the same values for the mean and variance which are represented by η_1, σ_1^2. We do not write the exact expressions for the above mean and variances because they can be simply obtained from (10) and (11). Finally, considering the threshold value i_{th} (Fig. 2), we can write the error probability as

$$Pe = \frac{1}{4}Q\left(\frac{\eta_{0,1} - i_{th}}{\sigma_{0,1}}\right) + \frac{1}{4}Q\left(\frac{\eta_{0,2} - i_{th}}{\sigma_{0,2}}\right) + \frac{1}{2}Q\left(\frac{i_{th} - \eta_1}{\sigma_1}\right) \tag{13}$$

where $Q(x) = 1/\sqrt{2\pi}\int_x^{+\infty} \exp(-y^2/2)\mathrm{d}y$.

5 Optical receiver performance evaluation

Assume that the input electrical field is

$$x(t) = A(t)\mathrm{e}^{-j(\omega t + \varphi(t))} + z(t) \tag{14}$$

where $z(t)$ represents an additive noise. In general, $z(t)$ is a zero mean noise with variance σ_z^2 that can be determined from the laser intensity noise characteristics see the appendix. At the first step, we consider $\varphi(t)$ as a deterministic value and derive the error probability which is conditioned on $\varphi(t)$, then we will obtain the total error probability by averaging over $\varphi(t)$.

Substituting (14) in (3) and using (4) and (5) we achieve the following equation

$$i_b(t) = R\Big[A(t)A(t-T)\cos(\varphi(t) - \varphi(t-T)) + z(t)z(t-T) + z(t)A(t-T)\mathrm{e}^{\mathrm{j}\varphi(t-T)} + z(t-T)A(t)\mathrm{e}^{\mathrm{j}\varphi(t)}\Big] \tag{15}$$

From Fig. 3, the decision variable is equal to

$$D_v = \int_0^T i_b(t)\mathrm{d}t \tag{16}$$

After substituting (15) in (16) we can obtain the mean value of D_v

$$\eta = R\int_0^T A(t)A(t-T)\cos(\varphi(t)-\varphi(t-T))\mathrm{d}t \quad (17)$$

Considering (15) we can also obtain the variance of $i_b(t)$. This variance is due to $z(t)$ and is equal to

$$\sigma_P^2 = R^2\sigma_z^2\left[\sigma_z^2 + A(t-T) + A(t)\right] \quad (18)$$

Considering the shot noise $\sigma_s^2 = eE\left[i_1(t)\right] + eE\left[i_2(t)\right]$ [10], and thermal noise σ_t^2, the total variance of $i_b(t)$ is equal to $\sigma_P^2 + \sigma_s^2 + \sigma_t^2$. As mentioned in Section 4, we assume that all noises are white. Therefore the variance of decision variable can be expressed as

$$\sigma^2 = \int_0^T \left[R^2\sigma_z^2\left[\sigma_z^2 + A(t-T) + A(t)\right] + \frac{eR}{2}\left[A^2(t) + A^2(t-T) + 2\sigma_z^2\right] + \frac{2kT_r}{r}\right]\mathrm{d}t \quad (19)$$

In order to obtain the error probability, we follow the same procedure as Section 4. Once again if the data bit is zero two cases may occur, then the corresponding means and variances are denoted by $\eta_{0,1}$, $\sigma_{0,1}^2$, $\eta_{0,2}$, $\sigma_{0,2}^2$ and if the data bit is one, then the other two cases may occur. Both of the above cases lead to the same mean and variance which are denoted by η_1, σ_1^2. Using (13), we can obtain the error probability which is conditioned on the phase value $\varphi(t)$. Now, we can take the impact of phase noise into account. The phase noise can be modelled as a Weiner–Levy random process [12] whose mean, variance and probability density function are as follows

$$E[\varphi(t)] = 0,\ \mathrm{VAR}[\varphi(t)] = \alpha t,\quad P[\varphi(t)] = \frac{1}{\sqrt{2\pi\alpha t}}\mathrm{e}^{-(\varphi^2(t)/2\alpha t)} \quad (20)$$

where α is the constant value which is related to the laser coherence time T_{coh}; $\alpha = 2/T_{coh}$ [13]. Considering (19), it can be easily verified that $\sigma_{0,1}^2$, $\sigma_{0,2}^2$ and σ_1^2 are independent from $\varphi(t)$. Therefore we consider only the mean values as random variable whose means and variances need to be calculated. Averaging (17) with respect to $\varphi(t)$ we can write

$$E[\eta] = R\int_0^T A(t)A(t-T) \times E\left[\frac{\mathrm{e}^{\mathrm{j}(\varphi(t)-\varphi(t-T))} + \mathrm{e}^{-\mathrm{j}(\varphi(t)-\varphi(t-T))}}{2}\right]\mathrm{d}t \quad (21)$$

Using (20) and Gaussian moment generating function, the above equation can be expressed as

$$E[\eta] = \mathrm{e}^{-\alpha T/2}\int_0^T A(t)A(t-T)\cos\left(\varphi_0(t)\right)\mathrm{d}t \quad (22)$$

where $\varphi_0(t)$ represents the deterministic phase difference between the successive transmitted bits, and it is caused by the chirp effect of the laser diode. In differential systems, if the value of transmitted bit is zero, the two successive transmitted waveforms will be similar, so the laser chirp have the same impact on both of them and $\varphi_0(t) = 0$, but if the value of transmitted bit is one, the two successive transmitted waveforms will have opposite signs so $\varphi_0(t) \neq 0$. Therefore the cosine term increases the difference between zero and one in differential UWB over fibre systems. Hence, it increases the Hamming distance and decreases the error probability.

In order to obtain the variance of η, we first derive $E\left[\eta^2\right]$ from (17). After a straightforward algebra, we achieve the following equation

$$E\left[\eta^2\right] = \frac{1}{2}\int_0^T\int_0^T A(t')A(t'-T)A(t)A(t-T) \times E\left[\cos\left(\varphi(t)-\varphi(t-T)+\varphi(t')-\varphi(t'-T)\right) + \cos\left(\varphi(t)-\varphi(t-T)-\varphi(t')+\varphi(t'-T)\right)\right]\mathrm{d}t\,\mathrm{d}t' \quad (23)$$

With no loss of generality, assume that $t' > t$. Fig. 6 shows the phase noise against time relations for $\varphi_0(t) = 0$; and we can deduce the following relations

$$\varphi(t'-T) = \varphi(t-T) + \varphi_1 \quad (24)$$

$$\varphi(t) = \varphi(t-T) + \varphi_1 + \varphi_2 + \varphi_0(t) \quad (25)$$

$$\varphi(t') = \varphi(t-T) + \varphi_1 + \varphi_2 + \varphi_3 + \varphi_0(t') \quad (26)$$

where $\varphi_3 = \varphi(t') - \varphi(t)$, $\varphi_2 = \varphi(t) - \varphi(t'-T)$, $\varphi_1 = \varphi(t'-T) - \varphi(t-T)$. Since the Weiner–Levy process is incrementally independent, φ_1, φ_2, φ_3 are independent, and their statistical characteristics are as follows

$$E\left[\varphi_1\right] = E\left[\varphi_2\right] = E\left[\varphi_3\right] = 0 \quad (27)$$

$$\mathrm{VAR}\left[\varphi_1\right] = \alpha(t'-t),\quad \mathrm{VAR}\left[\varphi_2\right] = \alpha(t'+T-t),\quad \mathrm{VAR}\left[\varphi_3\right] = \alpha(t'-t) \quad (28)$$

Substituting (24)–(26) in (23), and using (27), (28) and considering the independence of φ_1, φ_2, φ_3 one can achieve the following result

$$E\left[\eta^2\right] = \frac{1}{2}\int_0^T\left[\int_t^T A(t')A(t'-T)A(t)A(t-T) \times \left\{\mathrm{e}^{-\alpha\left[2(t'-t)+T\right]}\cos\left(\varphi_0(t)+\varphi_0(t')\right)\right.\right.$$

doi: 10.1049/iet-com:20080124

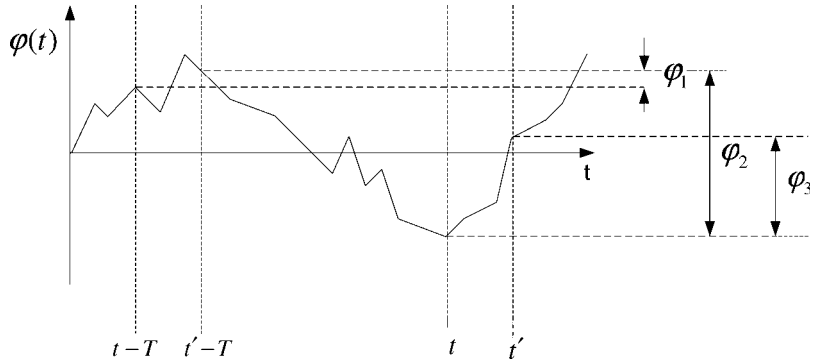

Figure 6 *Phase noise against time*

$$+e^{-\alpha[t'-t]}\cos\left(-\varphi_0(t)+\varphi_0(t')\right)\Big\}dt'$$
$$+\int_0^t A(t')A(t'-T)A(t)A(t-T)$$
$$\times\left\{e^{-\alpha[2(t-t')+T]}\cos\left(\varphi_0(t)+\varphi_0(t')\right)\right.$$
$$\left.+e^{-\alpha[t-t']}\cos\left(-\varphi_0(t)+\varphi_0(t')\right)\right\}dt'\Big]dt \qquad (29)$$

The variance of η can be simply obtained from (22) and (29) $(\mathrm{VAR}[\eta]=E[\eta^2]-E^2[\eta])$.

Substituting $A(t)=A(t-T)=A_b\pm A_m u(t)$ in (22) and (29), we obtain $E[\eta_{0,1}]$, $E[\eta_{0,2}]$, $\mathrm{VAR}[\eta_{0,1}]$, $\mathrm{VAR}[\eta_{0,2}]$, and substituting $A(t)=A_b+A_m u(t)$, $A(t-T)=A_b-A_m u(t)$ in (22) and (29), we obtain $E[\eta_1]$ and $\mathrm{VAR}[\eta_1]$. Using these values, the total error probability is obtained by averaging the conditional error probability and is expressed as

$$Pe=\frac{1}{4}\int_{-\infty}^{+\infty}Q\left(\frac{\eta_{0,1}-i_{th}}{\sigma_{0,1}}\right)\frac{1}{\sqrt{2\pi\mathrm{VAR}[\eta_{0,1}]}}$$
$$\times\exp\left(-\frac{(\eta_{0,1}-E[\eta_{0,1}])^2}{2\mathrm{VAR}[\eta_{0,1}]}\right)d\eta_{0,1}$$
$$+\frac{1}{4}\int_{-\infty}^{+\infty}Q\left(\frac{\eta_{0,2}-i_{th}}{\sigma_{0,2}}\right)\frac{1}{\sqrt{2\pi\mathrm{VAR}[\eta_{0,2}]}}$$
$$\times\exp\left(-\frac{(\eta_{0,2}-E[\eta_{0,2}])^2}{2\mathrm{VAR}[\eta_{0,2}]}\right)d\eta_{0,2}$$
$$+\frac{1}{2}\int_{-\infty}^{+\infty}Q\left(\frac{i_{th}-\eta_1}{\sigma_1}\right)\frac{1}{\sqrt{2\pi\mathrm{VAR}[\eta_1]}}$$
$$\times\exp\left(-\frac{(\eta_1-E[\eta_1])^2}{2\mathrm{VAR}[\eta_1]}\right)d\eta_1 \qquad (30)$$

6 Numerical results

In this section, we use the mathematical models of Section 2 to obtain the waveforms at the receiver, then using the analytical expressions of the error probability, which are derived in Sections 4 and 5, we calculate the performance of the whole system shown in Fig. 1. We assume that the length of the SMF is 4 km which leads to 0.8 dB attenuation. The duration of UWB signals are ~200 ps. The bit duration is 2 ns for Figs. 7–11. Fig. 12 shows how the duration of UWB signal is different from bit duration. The coherence time of the DFB laser is 32 ns for Fig. 7, and the DFB laser RIN is equal to −135 dB/Hz for all figures. These values are typical values which are selected for simulation purposes and they are not measured. The target bit error rate is 10^{-5} that corresponds to the packet error rate of 10^{-2} [14].

Fig. 7 shows the error probability of the optical receiver against the modulating power. Each line corresponds to a specific bias power corresponding a specific bias current. Note that P_b and P_m are introduced in Section 2. As expected when the modulating power increases, the error probability decreases. It can also be observed that larger bias powers cause larger bit error probability. The reason is evident from (29). Considering this equation, it can be realised that increasing the bias power increases the variance of phase noise which is the dominant noise for the optical receiver.

Note that the coherence time of the laser is the same, 32 ns, for all points in Fig. 7. If the coherence time is increased the phase noise will be reduced. Therefore larger values for coherence time lead to lower error probabilities, this can be verified by observing Fig. 8 in which the error probability of the optical receiver is sketched against the modulating power, P_m, for various values of the coherence time and optical bias power, P_b.

Fig. 9 shows the performance of the electrical receiver. In this figure, the impact of bias power and wireless channel fading is investigated. IEEE 802.15.3a UWB channel model is used to model the wireless channel fading

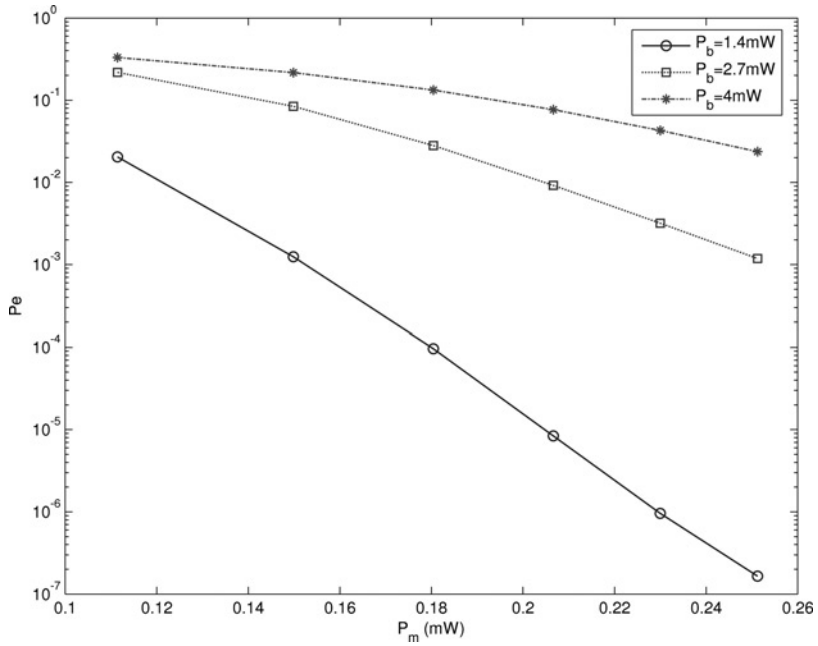

Figure 7 *Error probability of optical receiver for various values of the bias power*

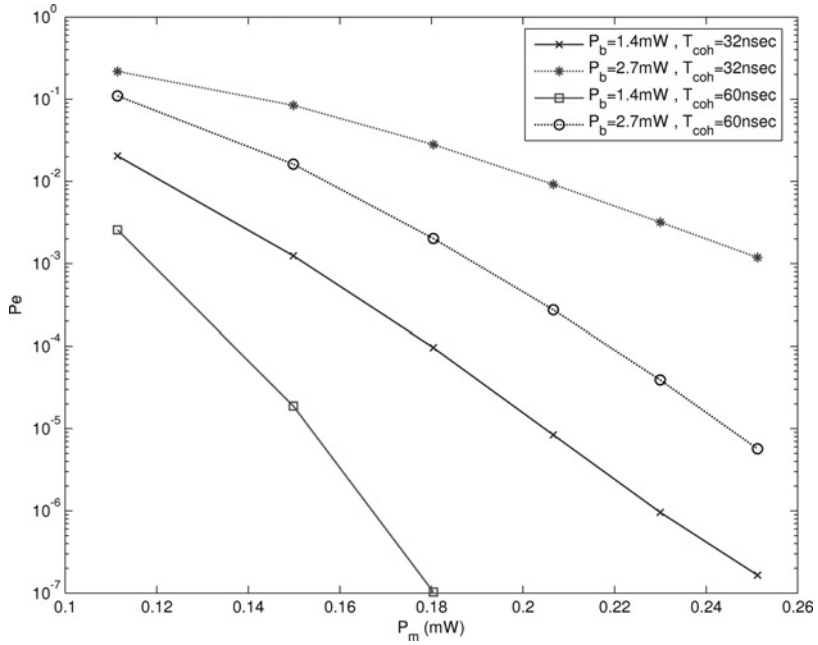

Figure 8 *Error probability of the optical receiver for various bias powers and various coherence times*

[15, 16]. In this model, four different measurement environments are defined namely CM1, CM2, CM3 and CM4. In this paper, we have considered CM1 which describes a line-of-sight scenario with a separation between transmitter and receiver of <4 m [15]. In order to consider the impact of fading, we have used the simulation method instead of analytical methods. We have simulated the wireless channel many times. Each time the corresponding impulse response is used to obtain $u(t)$, and the corresponding error probability is obtained using (13). The final error probability is obtained by averaging over many wireless channel states.

From Fig. 9, it can be realised that fading degrades the performance of the system, but the effect of bias power is more serious. In fact, since the coherence time of wireless channel, 200 μs [14], is usually much larger than the bit duration, the wireless channel is the same for the two successive bits, so the differential receiver can collect the total energy distributed in the multipath signal. That is why, the

doi: 10.1049/iet-com:20080124

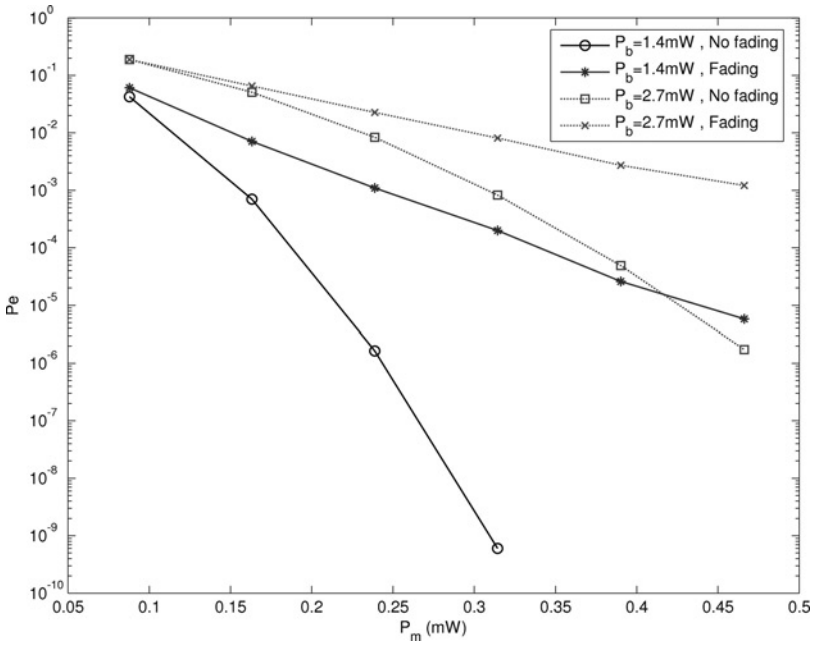

Figure 9 *Error probability of the electrical receiver for various bias powers and fading levels*

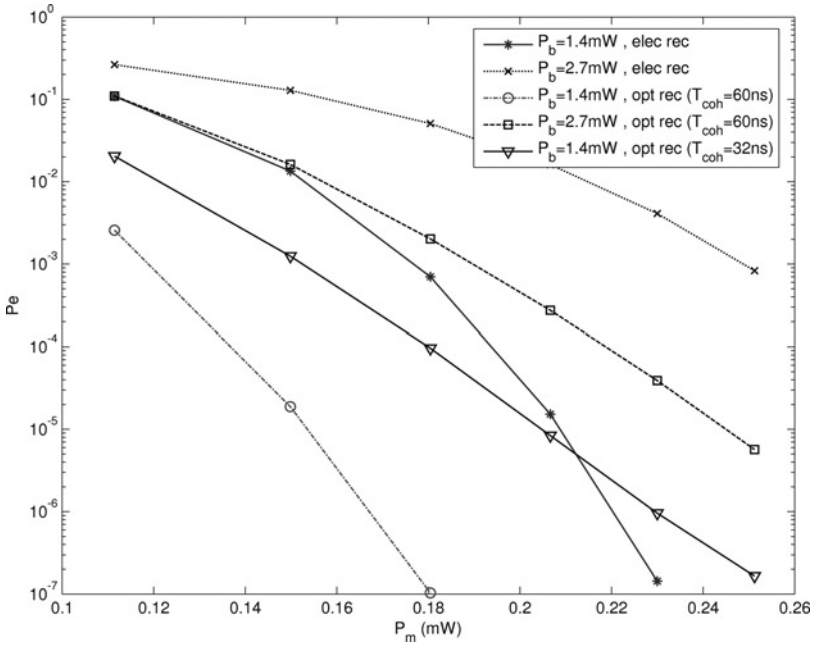

Figure 10 *Performance comparison between the electrical receiver and the optical receiver*

impact of the fading on the performance is not very much. Note that we have assumed that the bit duration is 40 ns which is large enough in order not to result in significant inter symbol interference [14, 15], and most of the energy distributed among various multipath components is collected. In the optical receiver, the coherence time of the laser must be much larger than the bit duration, otherwise the phase noise will be very strong and the performance degrades seriously. Therefore a system with a large bit duration requires a laser diode with a large coherence time. For example, the coherence time of a typical DFB laser is around 32 ns which is even less than the bit duration, 40 ns. Therefore it is not possible to use such a DFB laser for this system, and a laser diode with larger coherence time must be used. DFB laser diodes with larger coherence time such as 600 ns are available widely [17]. Using such DFB lasers, the bit duration can be as much as 40 ns without any significant performance degradation. On the other hand, master-slave structured DFB laser diodes with the coherence time of the order of 20 μs are also reported in literature [18]. Therefore it seems that using such laser diodes, bit durations as much as tens of microsecond can be supported with the optical receiver. However,

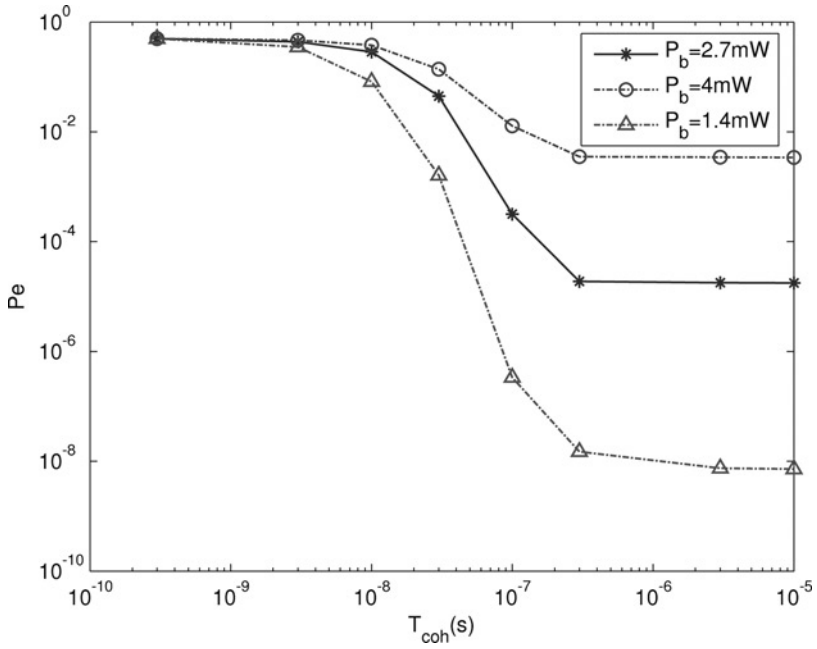

Figure 11 *Error probability of the optical receiver against the laser coherence time*

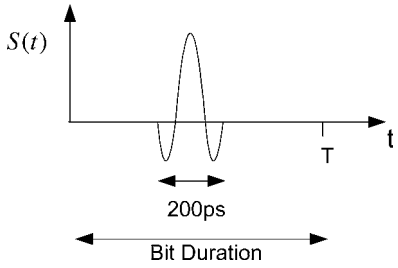

Figure 12 *Bit duration and the duration of UWB signal (200 ps)*

implementing large bit duration systems requires long fibre lengths in the Mach–Zehnder interferometer (Fig. 3) as stated in Section 2. This problem limits the maximum supportable bit duration to tens of nanosecond.

In Fig. 10, the performance of the optical receiver and the electrical receiver are compared. In order to have a more instructive comparison, the effect of the bias power and the laser coherence time is also examined in this figure. From this figure, it can be realised that the optical receiver with the coherence time of 60 ns outperforms the electrical receiver (for both bias powers of 1.4 and 2.7 mW). However, the performance of the optical receiver severely depends on the laser coherence time, whereas the performance of the electrical receiver is independent from the coherence time. For example, compare the error probability of electrical receiver ($P_b = 1.4$ mW) with that of optical receiver ($P_b = 1.4$ mW, $T_{coh} = 32$ ns). In this case, unlike the case of $T_{coh} = 60$ ns, the performance of optical receiver and the electrical receiver are close and the optical receiver error probability crosses that of the electrical receiver. The electrical receiver outperforms the optical receiver for large values of modulating power. The reason is that the phase noise variance is less sensitive to the modulating power value compared with other noises. However, 32 ns is a typical value for the DFB laser coherence time and we can conclude that the performance of optical receiver and electrical receiver are similar for the bit duration of 2 ns and a typical DFB laser.

In Fig. 11, the error probability of optical receiver is plotted against the laser coherence time. The modulating power is 0.14 mW and the bit duration is 2 ns in this figure. As expected, and as it can be realised from this figure, the error probability decreases when the coherence time is increased. However, for each bias power, there is a floor value for the error probability which is almost constant for the coherence time values exceeding 300 ns. This can be explained as follows; when the coherence time increases, the variance of phase noise decreases so that the phase noise is no longer the dominant noise for coherence time values that are large enough. In this case, other noises such as shot noise, thermal noise or intensity noise become the dominant noise and errors are mostly caused by such noises which are independent from the laser coherence time. As discussed before, DFB lasers with coherence time value larger than 300 ns are available [17]. Using these DFB lasers, we obtain the performance limit of the optical receiver for a small bit duration such as 2 ns which is used in this figure.

7 Conclusions

In this paper, we studied the transmission of differential IR-UWB signals over SMF. We studied an optical receiver structure for the fist time in this application as well as the conventional electrical receiver. We observed that the

doi: 10.1049/iet-com:20080124

increase of laser diode bias current degrades the performance of receivers. We also compared electrical and optical receivers and showed that the performance of optical receiver severely depends on the laser diode coherence time, but it is close to that of the electrical receiver for typical and practical UWB bit rates (500 Mb/s) and viable DFB lasers ($T_{coh} = 32$ ns). The optical receiver can also outperform the electrical receiver for larger values of coherence time (e.g. $T_{coh} = 60$ ns for the bit rate of 500 Mb/s), but when the laser coherence time is small compared with the bit duration the performance of the optical receiver degrades seriously.

8 Acknowledgment

The work has been supported by Iran National Science Foundation (INSF).

9 References

[1] GHAVAMI M., MICHAEL L.B., KOHNO R.: 'Ultra wide band signals and systems in communication engineering' (Wiley, 2004, 1st edn.)

[2] TAN C.M., ONG L.C., YEE M.L., LUO B., TANG P.K.: 'Direct transmission of ultra wide band signals using single mode radio-over-fiber system'. Microwave Conf. Proc., APMC, Asia-Pacific, December 2005, vol. 2, p. 3

[3] LIM C.S., YEE M.L., ONG C.L.: 'Performance of transmission of ultra wideband signals using radio-over-fiber system'. Proc. 6th Int. Conf. ITS Telecommunications, June 2006, pp. 250–253

[4] WAH M.Y., YEE C., YEE M.L.: 'Wireless ultra wideband communications using radio over fiber'. 2003 IEEE Conf. Ultra Wideband Systems and Technologies, November 2003, pp. 265–269

[5] YANG L., GIANNAKIS G.B.: 'Ultra-wideband communications an idea whose time has come', *IEEE Signal Process. Mag.*, 2004, **21**, (6), pp. 26–54

[6] BATRA A., BALAKRISHNAN J., DABAK A.: 'Multi-band OFDM: a new approach for UWB'. Proc. 2004 Int. Symp. Circuits and Systems (ISCAS), 2004, vol. 5, V-365–V-368

[7] BOSCI G., POGGIOLINI P.: 'The impact of receiver imperfections on the performance of optical direct-detection DPSK', *J. Lightw. Technol.*, 2005, **23**, (2), pp. 842–848

[8] MADSEN C.K., ZHAO J.H.: 'Optical filter design and analysis: a signal processing approach' (Wiley, 1999, 1st edn.)

[9] CABON B., JAZAYERIFAR M., NGUYEN G.: 'RoF techniques for broadband access'. IEEE Radio and Wireless Symp. RWS2008 Workshop WM2: Radio over Fiber Technologies, Orlando, USA, January 2008, pp. 21–24

[10] AGRAWAL G.E.: 'Fiber-optic communication systems' (Wiley, 2002, 2nd edn.)

[11] CARTLEDGE J., SRINIVASAN R.C.: 'Extraction of DFB laser rate equation parameters for system simulation purposes', *J. Lightw. Technol.*, 1997, **15**, (5), pp. 852–860

[12] MANSOURI-RAD M., SALEHI J.A.: 'Phase-induced intensity noise in digital incoherent all-optical tapped-delay line systems', *J. Lightw. Technol.*, 2006, **24**, (8), pp. 3059–3072

[13] SALEHI M.R., CABON B.: 'Theoretical and experimental analysis of influence of phase-to-intensity noise conversion in interferometric systems', *J. Lightw. Technol.*, 2004, **22**, (6), pp. 1510–1518

[14] IEEE P 802.15 Working Group for Wireless Personal Area Networks (WPANs), UWB Channel Modeling Contribution from Intel, June 2002

[15] FOERSTER J.R., PENDERGRASS M., MOLISCH A.F.: 'A UWB channel model for ultra wideband indoor communications'. Proc. Int. Symp. Wireless Personal Multimedia Communications (WPMC), October 2003

[16] www.mathworks.com/matlabcentral (available at January 2008)

[17] Single-mode DFB laser diode: www.mitsubishichips.com

[18] LISSILLOUR F., GABET R., FÉRON P., BESNARD P., STÉPHAN G.: 'Linewidth narrowing of a DFB semiconductor laser at 1.55 μm by optical injection of an Er: ZBLAN microspherical laser', *Europhys. Lett.*, 2001, **55**, (4), pp. 499–504

9 Appendix

In this appendix, we express the field noise against the intensity noise. Assume that the received electrical field is $y(t) + z(t)$, where $z(t)$ represents the additive zero mean noise. The photo-detected electrical current will be as follows

$$i(t) = R\left|y(t) + z(t)\right|^2 \tag{31}$$

The variance of $i(t)$ is obtained after some algebra

$$\mathrm{VAR}\{i(t)\} = R^2\left(2\sigma^4 + 4\sigma^2 y^2(t)\right) \tag{32}$$

where σ^2 is the variance of $z(t)$. The intensity of noise is usually much weaker than that of the received signal when the system is in the normal mode of operation. Therefore the first term in (32) can be neglected compared with the

second term

$$\mathrm{VAR}\{i(t)\} \simeq R^2\left(4\sigma^2 y^2(t)\right) \tag{33}$$

On the other hand, the variance of $i(t)$ can be expressed in terms of the intensity noise specifications [10]

$$\mathrm{VAR}\{i(t)\} = R^2 P_o^2(t)(\mathrm{RIN}) \tag{34}$$

where $P_o(t)$ is the received optical power. Comparing (33) and (34) and noting that $P_o(t) = y^2(t)$ one can simply achieve the following equation

$$\sigma^2 = P_o(t)(\mathrm{RIN})/4 \tag{35}$$

The above equation expresses the variance of $z(t)$ against the intensity noise.

doi: 10.1049/iet-com:20080124